Brain Research 1752 (2021) 147221

Contents lists available at ScienceDirect

Brain Research

journal homepage: www.elsevier.com/locate/brainres

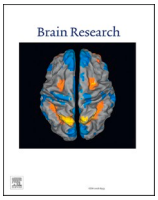

Effect of muscle fatigue on the cortical-muscle network: A combined electroencephalogram and electromyogram study

Xugang Xi [a,b,*], Shaojun Pi [a,b], Yun-Bo Zhao [c], Huijiao Wang [d], Zhizeng Luo [a,b,*]

[a] School of Artificial Intelligence, Hangzhou Dianzi University, Hangzhou 310018, China
[b] Key Laboratory of Brain Machine Collaborative Intelligence of Zhejiang Province, Hangzhou 310018, China
[c] Department of Automation, Zhejiang University of Technology, Hangzhou 310023, China
[d] Hangzhou Vocational & Technology College, Hangzhou 310018, China

ARTICLE INFO

Keywords:
Muscle fatigue
Symbolic transfer entropy
Cortical-muscle network
Electroencephalogram
Electromyogram

ABSTRACT

Electroencephalogram (EEG) and electromyogram (EMG) signals during motion control reflect the interaction between the cortex and muscle. Therefore, dynamic information regarding the cortical-muscle system is of significance for the evaluation of muscle fatigue. We treated the cortex and muscle as a whole system and then applied graph theory and symbolic transfer entropy to establish an effective cortical-muscle network in the beta band (12–30 Hz) and the gamma band (30–45 Hz). Ten healthy volunteers were recruited to participate in the isometric contraction at the level of 30% maximal voluntary contraction. Pre- and post-fatigue EEG and EMG data were recorded. According to the Borg scale, only data with an index greater than 14<19 were selected as fatigue data. The results show that after muscle fatigue: (1) the decrease in the force-generating capacity leads to an increase in STE of the cortical-muscle system; (2) increases of dynamic forces in fatigue leads to a shift from the beta band to gamma band in the activity of the cortical-muscle network; (3) the areas of the frontal and parietal lobes involved in muscle activation within the ipsilateral hemibrain have a compensatory role. Classification based on support vector machine algorithm showed that the accuracy is improved compared to the brain network. These results illustrate the regulation mechanism of the cortical-muscle system during the development of muscle fatigue, and reveal the great potential of the cortical-muscle network in analyzing motor tasks.

1. Introduction

Muscle fatigue is defined as a decline in the ability to maintain a certain level of strength during continuous contraction, or failure to reach the initial strength level during intermittent contraction, which is reflected in the electrical activity of the muscle (Ament and Verkerke, 2009). This term indicates the feeling that it is more difficult than the expected or requires more effort. For healthy people, repetitive or continuous muscle activation will result in fatigue, which is common in exercise or daily life. The most intuitive effects is the decrease in the muscle's ability to produce force, which increases the likelihood of muscle injury. This performance is also closely related to patients with motor dysfunction, such as stroke and cancer. Hence, it is of utmost importance to understand and assess muscle fatigue effectively and accurately.

Since the relationship between electroencephalogram (EEG) and electromyogram (EMG) during motion was first identified (Conway et al., 1995), dynamic cortical-muscle communication has become an important research topic. Cortical-muscle coherence (CMC) is closely related to body motion (Belardinelli et al., 2017; Yoshida et al., 2017). The same research interest has also been applied to muscle fatigue (Yang et al., 2009) that CMC decreased after maximum voluntary contraction-induced fatigue. Subsequently, they optimized the experimental paradigm based on the fact that fatigue is a progressive process, and reached the same conclusion (Yang et al., 2010). In contrast, a recent study (Martínez-Aguilar and Gutiérrez, 2019) set individual fatigue thresholds for volunteers and found CMC to both increase and decrease. This may reflect the subject's ability to continue after the onset of fatigue. Meanwhile, the reduction in the power of EEG and EMG (Liu et al., 2005), the reduction in the coherence of EEG (Di Fronso et al., 2018), and the increase in EMG cyclostationarity (Karthick et al., 2016) have also been reported. Inconsistent conclusions are likely to be the result of two limitations of these studies, related to the direction of information flow of the cortical-muscle network (Mima et al., 2000), and the fact that

* Corresponding authors at: School of Artificial Intelligence, Hangzhou Dianzi University, Hangzhou 310018, China.
E-mail addresses: xixi@hdu.edu.cn (X. Xi), luo@hdu.edu.cn (Z. Luo).

https://doi.org/10.1016/j.brainres.2020.147221
Received 14 September 2020; Received in revised form 14 November 2020; Accepted 28 November 2020
Available online 23 December 2020

both the brain and muscle are involved in the development of fatigue (Gandevia, 2001). Stroke research shows that, in CMC, commands are transmitted through communication, not sensory feedback (Mima et al., 2001). In addition, exercise is coordinated by multiple brain regions and muscles, and the brain and muscle groups form a complex system composed of hundreds of billions of neurons (Baars and Gage, 2010).

To improve knowledge in the above topic, for the first time, we propose a method to establish the cortical-muscle network by combining symbolic transfer entropy (STE) (Staniek and Lehnertz, 2008) and graph theory (Strogatz, 2001) to investigate muscle fatigue. Owing to the asymmetry (directed) and process (dynamic) probability calculations, the STE method is particularly effective in detecting nonlinear interactions (Staniek and Lehnertz, 2008) and has been previously applied to EEG and EMG signals (Gao et al., 2018; Yao and Wang, 2017). Graph theory provides a powerful method for quantitative research on brain network organization (Wang et al., 2018). Network characteristics such as shortest path length, clustering coefficient, efficiency, and small-world property are used to describe the network (Sheffield et al., 2017). Communication dynamics may act as potential generative models of effective connectivity and can offer insight into the mechanisms by which brain networks transform and process information (Avena-Koenigsberger et al., 2018). When the combination of graph theory and STE acts on EEG/EMG, the outcome is a network with nodes as EEG and EMG channels, and the edge represents the directed coupling strength between the channels.

Moreover, it is necessary to validate the proposed method by training the classifier with the extracted cortical-muscle network characteristics and distinguishing whether fatigue. In this study, we adopted a support vector machine (SVM) algorithm to train a classifier, and to identify whether the muscle is in a fatigue state.

2. Results

2.1. Adjacency matrices

Weighted directed adjacency matrices were first obtained by STE for the beta and gamma bands within each state. Fig. 1 shows the grand average connectivity matrices for the pre-fatigue and post-fatigue periods. With respect to muscle fatigue, the average STE in the adjacency matrix increases. The paired-Student's *t*-test was conducted to identify significant differences between the two states across all frequency bands. The results indicated that STE within the beta band showed no significant differences ($p = 0.54$), but significant differences in the gamma band were observed ($p = 0.04$). Fig. 2 shows the binary network of individual subject in a single experiment, converted from a weighted adjacency matrix based on cost efficiency. The effective connection between nodes are represented by lines, and the direction is expressed as a line from thin to thick. The statistical analysis results showed that after fatigue, the network connection in the beta frequency band becomes sparse ($p = 0.03$), while the network connection in the gamma frequency band becomes tighter ($p = 0.007$).

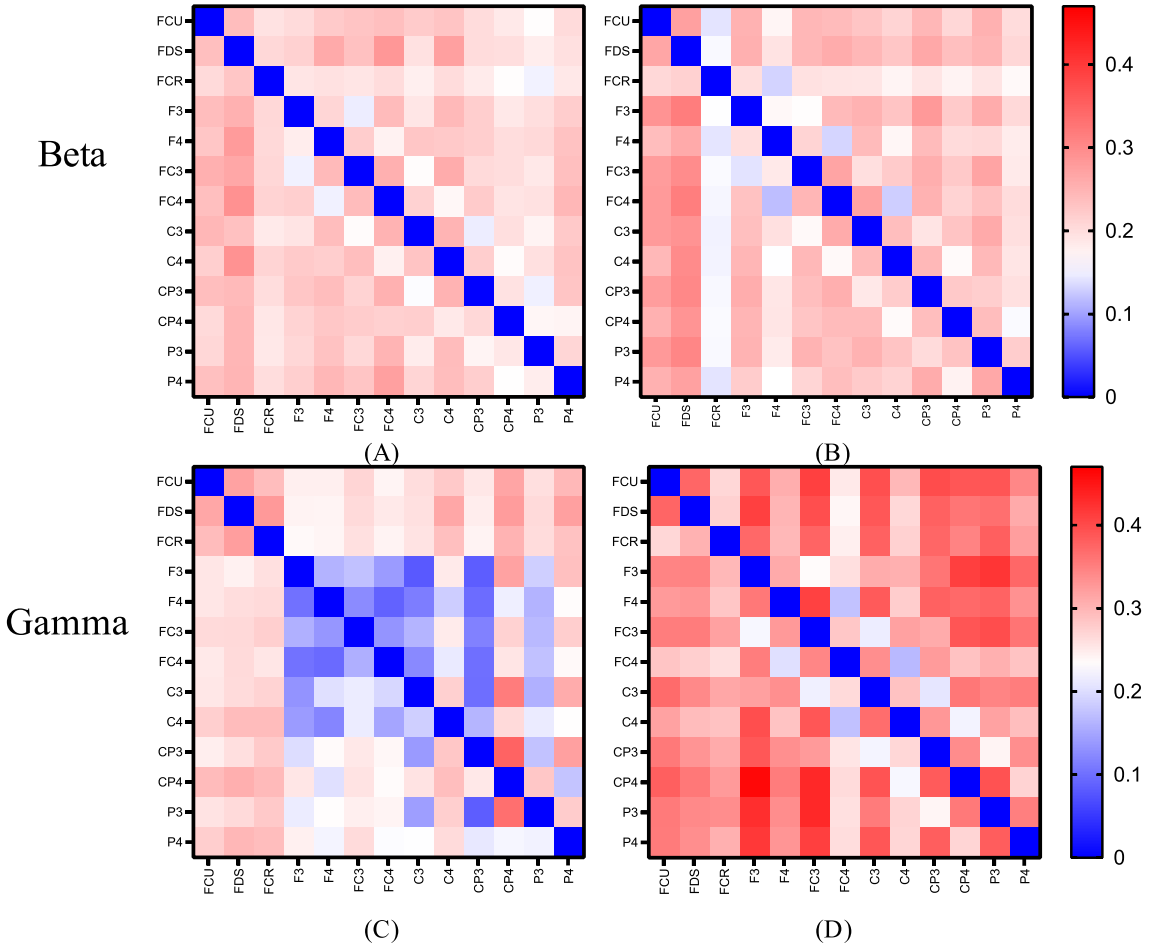

Fig. 1. Group-average adjacency matrices. (A) Group-average adjacency matrix during pre-fatigue in the beta band; (B) Group-average adjacency matrix during post-fatigue in the beta band; (C) Group-average adjacency matrix during pre-fatigue in the gamma band; (D) Group-average adjacency matrix during post-fatigue in the gamma band. For all, the element in the matrix such as (C3, FDS) represents the STE value from C3 to FDS.

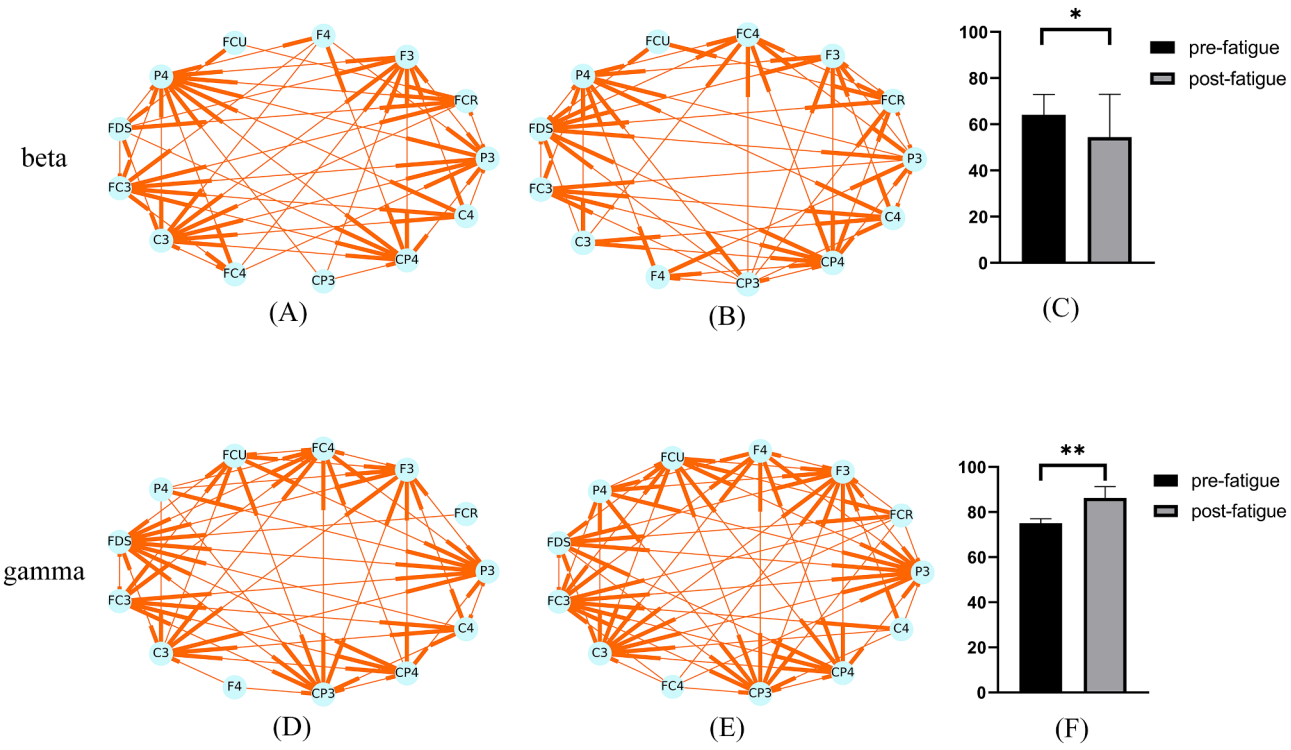

Fig. 2. Network presentation and statistical analysis results. (A) Network presentation during pre-fatigue in the beta band; (B) Network presentation during post-fatigue in the beta band; (C) Group-average number of network edges in the beta band; (D) Network presentation during pre-fatigue in the gamma band; (E) Network presentation during post-fatigue in the gamma band; (F) Group-average number of network edges in the gamma band. Each edge represents the direction; the thin section directed towards the thick section. For all, **p < 0.01, *p < 0.05.

2.2. Network characteristics

The average degree, local efficiency, and clustering coefficient of the cortical-muscle network are shown in Fig. 3(A, B and C), respectively. Significant differences ($p < 0.05$) before and after fatigue for each channel are marked.

A high in-degree is interpreted as a channel that accepts more information from other channels and is more likely to be affected by other channels, while a high out-degree means that this channel acts more as a functional target in the network. It is apparent from Fig. 3A that the average value of the in-degree and out-degree during the post-fatigue period was smaller than the pre-fatigue period in the beta band, while the gamma band showed the opposite, which was greater than in the pre-fatigue period. Paired Student's *t*-testing was performed further on the average degree of all nodes. There were no significant differences in the degrees of the beta band (in-degree: $p = 0.37$; out-degree: $p = 0.54$), but significant differences in the degrees of the gamma band were observed (in-degree: $p = 0.03$; out-degree: $p = 0.04$).

Local efficiency measures the local information transmission capability of the network and informs us about the fault-tolerance of the network system, while the clustering coefficient describes the degree of clustering between the channels in the network. Specifically, it is the degree of interconnection between adjacent channels of a channel. In Fig. 3(B and C), it is interesting to note that they show the same trend, like degrees: a decrease in the beta band, and an increase in the gamma band. Paired-Student's *t*-tests were also performed on the average of these two indexes of all nodes. The results showed significant differences for the factor group within each band (local efficiency: *p-beta* = 0.003, *p-gamma* < 0.001; clustering coefficient: *p-beta* = 0.02, *p-gamma* < 0.001).

Watts and Strogatz (1998) combined the shortest path length and the clustering coefficient to propose a small-world property. Here, to explore whether the effective cortical-muscle network established by taking the cortex and muscle as a whole is a small-world network, we applied small-world measurements to the analyzed network. Table 1 shows the summary result for all subjects, which indicate that the cortical-muscle networks are all a small-world network. A *t*-test was performed on the small-world property indexes to analyze the relationship between pre-fatigue and post-fatigue. There were no significant differences in the beta band ($p = 0.51$), but significant differences in the gamma band ($p = 0.03$).

2.3. Muscle fatigue recognition

To validate the feasibility of the proposed method, we performed muscle fatigue recognition in the beta band and the gamma band based on the extracted features. Table 2 shows the average recognition accuracy (AC) in the two frequency bands. It can be seen that, according to our proposed method, the average accuracy of beta band is 72.6%, and the average accuracy of gamma band is 81.7%; these values were higher than the corresponding values measured using the brain network method.

3. Discussion

The present study combined STE and graph theory to research the effective cortical-muscle network in healthy people under different muscle states. From the perspective of degree, local efficiency, clustering coefficient, and small-world property, we analyzed the differences between effective networks to explore the mechanisms of muscle fatigue. The results show that compared to the pre-fatigue period, the topology of the cortical-muscle network may present differences during fatigue.

Regarding the strengthening of STE, we propose a hypothesis that due to the ability of output force to decrease after fatigue (Wan et al., 2017), more effort is needed, which increases the force level indirectly. This hypothesis is in agreement with previous studies, wherein the CMC of the beta band and gamma band increased with an increase in the force

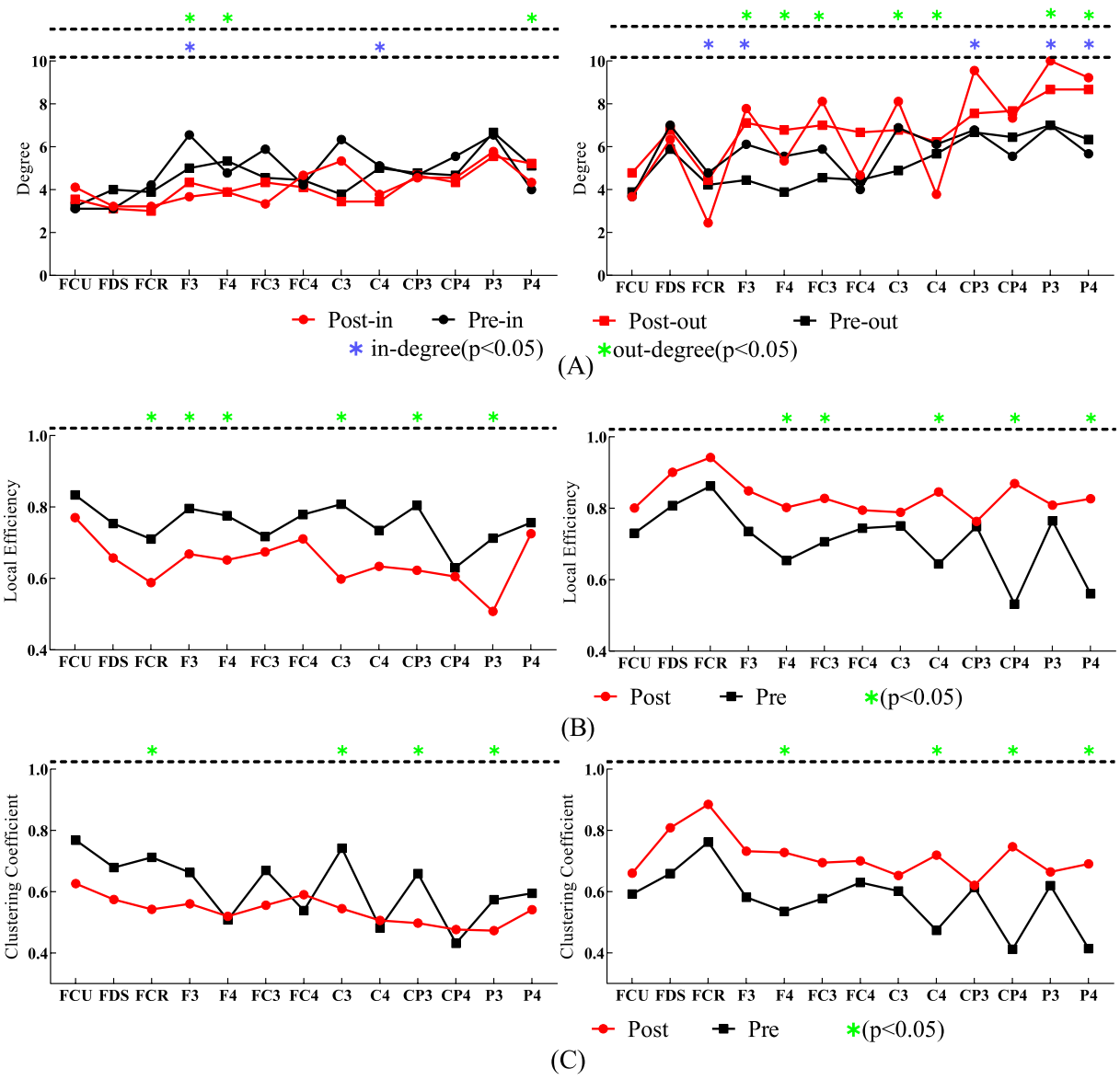

Fig. 3. Group-average Network characteristics in the beta band (left) and gamma band (right). (A) Group-average degree (in-degree and out-degree). Pre-in means in-degree during pre-fatigue, pre-out means out-degree during pre-fatigue, post-in means in-degree during post-fatigue and post-out means out-degree during post-fatigue; (B) Group-average local efficiency; (C) Group-average clustering coefficient. For all, the black line means during pre-fatigue and the red line means during post-fatigue, *p $<$ 0.05.

Table 1
Clustering coefficient, shortest path length, and small-world index in two muscle states of each subject.

	Beta						Gamma					
	Pre-fatigue			Post-fatigue			Pre-fatigue			Post-fatigue		
	C_{real}	L_{real}	σ	C_{real}	L_{real}	σ	C_{real}	L_{real}	σ	C_{real}	L_{real}	σ
S1	0.52	0.33	1.57	0.62	0.44	1.36	0.52	0.23	2.05	0.69	0.57	1.13
S2	0.53	0.27	1.98	0.56	0.29	1.91	0.62	0.29	1.98	0.72	0.56	1.20
S3	0.55	0.31	1.77	0.49	0.30	1.60	0.69	0.33	1.93	0.75	0.56	1.25
S4	0.72	0.42	1.66	0.57	0.35	1.61	0.66	0.39	1.59	0.50	0.35	1.32
S5	0.72	0.35	1.99	0.65	0.41	1.55	0.63	0.40	1.47	0.72	0.60	1.12
S6	0.60	0.38	1.54	0.56	0.34	1.59	0.58	0.48	1.13	0.78	0.62	1.17
S7	0.57	0.36	1.72	0.74	0.51	1.41	0.61	0.48	1.18	0.80	0.60	1.25
S8	0.65	0.41	1.37	0.71	0.40	1.75	0.73	0.51	1.32	0.79	0.45	1.64
S9	0.63	0.43	1.45	0.65	0.45	1.41	0.74	0.58	1.20	0.70	0.58	1.16
S10	0.57	0.31	1.80	0.66	0.40	1.61	0.70	0.39	1.67	0.67	0.60	1.04

C_{real} = Network clustering coefficient. L_{real} = Global shortest path length.σ = Small-world index.

Table 2
Comparison of the recognition performance in the proposed method and the brain network method.

Frequency	beta	gamma
AC-CMN (%)	72.6	81.7
AC-BN (%)	71.9	75.6

AC-CMN = Accuracy based on the cortical-muscle network. AC-BN = Accuracy based on the brain network.

level (Chakarov et al., 2009). Practically, it has been found by surface electromyographic decomposition technology that fatigue requires more motor units to participate (Contessa et al., 2016). Based on this, it is clear that more new motor units are recruited due to the decrease in the ability of output force, resulting in increased STE. A similar results (Wang et al., 2015) have also been reported that the coherence of EMG increases during sustained submaximal isometric contraction-induced fatigue. The increased STE may maintain force stability on the basis of maintaining the force output.

Our results show that the network characteristics show the same overall change trend. Under fatigue, the most obvious characteristics occur in the gamma band, and these characteristics are decreased in beta band while increased in the gamma band, which implies that muscle fatigue leads to the activity of the cortical-muscle network to shift from the beta band to the gamma band. We initially believed that this was due to the modulation of different forms of force by the cortical-muscle system. Because under static forces, significant coherence is limited to the beta band; whereas under dynamic forces, the most obvious coherence occurs in the gamma band, and the beta band coherence is significantly reduced (Omlor et al., 2007). However, the decrease in the beta band did not appear in the STE of our result. At this point, we hesitated to interpret these differences because the fatigue data we processed had more dynamic forces. Meanwhile, our results showed that the left hemibrain (especially F3, C3, and P3) had a higher overall in-degree. This suggests that a great amount of information flows from other brain regions. This means these brain regions may act as a "network navigation hub" in different muscle states. Deleting this node from the network is likely to lead to the whole cortical-muscle system to crash. More specifically, the muscle-activated contralateral hemibrain assumes more exercise control and planning responsibilities in maintaining the grip strength meter to reach the specified task.

The nodes with a high clustering coefficient act as activation centers. A distinct activation center existed in both the beta band and gamma band during the pre-fatigue period; as fatigue developed, the obvious activation center was limited to the gamma band, while no significant activation center was found in the beta band. It should be emphasized that in addition to the central region related to motion, the frontal and parietal lobes also appear in these changes in the clustering coefficient. Parietal lobe atrophy causes involuntary fatigue in patients (Pellicano et al., 2010), and the EEG power spectrum of the frontal lobe increased during long-term exercise at high temperature to exhaustion (Nielsen et al., 2001), which indicates the importance of parietal and frontal lobes during muscle fatigue. From this characteristic, we infer that the frontal and parietal lobes may play a compensatory role in fatigue. Although there is no direct connection, our results link the changes in the network topology and suggest that the frontal and parietal lobes of muscle activation in the ipsilateral hemibrain are related to the compensation mechanism in autonomous fatigue. However, it seems that we cannot explain how they compensate for fatigue here due to methodological limitations. Liu et al. (2007) found that the center of gravity of the EEG source moved to the muscle-activated anterior and lower cortical regions of the ipsilateral hemibrain. Our results provide evidence for the same phenomenon in the frontal and parietal lobes of the right hemibrain in the gamma band. This indicates that the cortical-muscle system will compensate for the decline in capacity in other regions, or greater demand due to fatigue by activating the frontal and parietal lobes of the right hemibrain. It should be noted that although there are differences in the activity of muscle groups before and after fatigue, the trend of the characteristic curve in muscle groups has not changed, which means that the muscle has more of a feedback role rather than being dominant. We also showed that the cortical-muscle networks established in this work presented a small-world network property like the brain network (Muldoon et al., 2016), which is characterized by a large clustering coefficient and a small shortest path length.

The proposed method increases the number of nodes compared to the brain function network, which consequently leads to an increase in the feature dimension. This may increase the redundant information in the feature matrix and reduce the recognition accuracy. However, the results show a slight increase in accuracy. The cortical-muscle network can still correctly reflect the characteristics of normal and fatigue states, which verifies the feasibility of the proposed method. In addition, the improvement of recognition accuracy also implies the great potential of cortical-muscle network research.

The current study has some limitations. First, only three EMG channels and ten EEG channels in the 64-channel acquisition device were selected; fewer channels may miss some movement-related areas, such as the occipital lobe (Busan et al., 2009), and some metrics are very sensitive to network size. Second, the choice of EEG signal frequency remains to be discussed. STE is an algorithm based on the time domain and can be applied to signals in different frequency ranges. In our analysis, only EEG and EMG signals of 12–45 Hz were considered, and the main frequency distribution of EMG was ignored at 45–150 Hz, which will result in the loss of some dynamic information from the EMG signals.

4. Conclusions

As far as we know, this is the first research to treat the cortex and muscle groups as a whole to establish an effective cortical-muscle network to analyze muscle fatigue. The results showed that both the connection strength and topology of the network changed after fatigue. The shifting from beta band to gamma band in the activity of the cortical-muscle network, and the compensatory role of the contralateral frontal and parietal lobe reveals a regulatory mechanism of human neurons on muscle fatigue, provides new insights and quantitative standards into the study of motion fatigue. Our work also implied the great potential of establishing a cortical-muscle network to analyze motion-related events. The method proposed in this study can be further applied to fatigue caused by some diseases, and it is expected to have an impact on the application of clinical research.

5. Material and methods

5.1. Overview

Fig. 4 provides an overview of the research workflow. After preprocessing EEG and EMG, STE was initially used to calculate the weighted directed adjacency matrix. Then, the threshold was determined to convert the weighted matrix to a binary matrix. Finally, the network characteristics were calculated for further analysis.

5.2. Experimental paradigm

In the experiment carried out in our study, ten right-handed volunteers from Hangzhou Dianzi University were recruited (2 women and 8 men; mean age, 23.4 years). Table 3 provides the demographic information of each subject. Subjects were excluded if they had neurological or musculoskeletal disorders, and/or consumption of illicit drugs, as well as head trauma. All subjects were required to provide written informed consent according to the Declaration of Helsinki, and the study was approved by the local ethics committee.

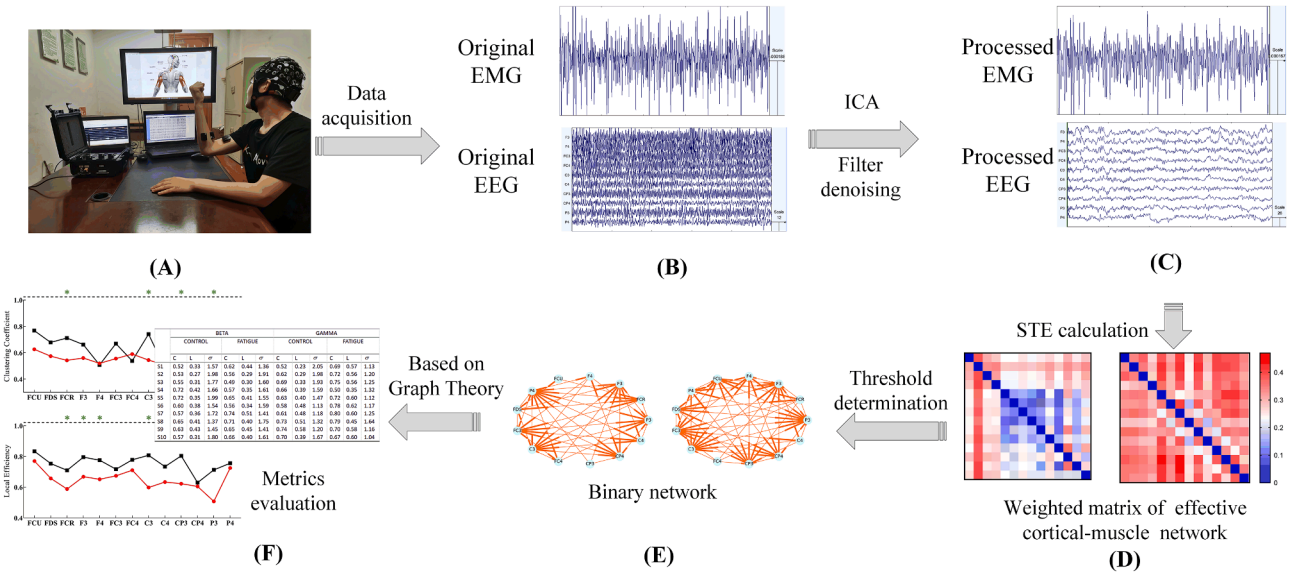

Fig. 4. Overview of the research workflow. (A) Presentation of experimental environment and subject posture; (B) Raw EEG and EMG data were recorded from electrodes; (C) Raw data were preprocessed and band-passed using the filter in two frequency bands: beta (12–30 Hz) and gamma (30–45 Hz); (D) Adjacency matrix calculated by symbolic transfer entropy; (E) Binary matrix after binarizing the adjacency matrix based on the determined threshold; (F) Network feature developed from the binary adjacency matrix.

Table 3
Demographic information and the Borg fatigue index of each subject.

Subject	Gender	Age	Dominant hand	MVC (kg)	BFI
S1	Female	21	Right	31.1	15 17 16 15 17 18 17 16 16 17
S2	Female	21	Right	27.9	15 16 18 16 17 19 18 18 16 16
S3	Male	23	Right	52.1	15 15 16 15 14 16 16 17 17 17
S4	Male	24	Right	45.3	15 17 16 15 17 15 15 16 17 18
S5	Male	24	Right	43.3	16 15 15 16 16 18 17 15 17 18
S6	Male	26	Right	53.1	16 15 17 15 15 16 17 17 19 18
S7	Male	24	Right	47.9	15 15 16 15 18 17 17 17 18 18
S8	Male	25	Right	48.0	15 16 15 16 17 18 17 17 18 17
S9	Male	23	Right	60.0	16 15 15 16 17 17 18 18 16 16
S10	Male	23	Right	49.4	16 15 15 17 17 16 16 15 17 17

MVC = Maximal voluntary contraction. BFI = Borg fatigue index.

Before the experiment began, the maximum grip strength of each subject was recorded. The subject was sitting in an electrically shielded room with their forearm placed on the table, while maintaining 30% maximal voluntary contraction (MVC) on the grip strength meter after an audio signal prompt (Fig. 5A). The experiment was divided into two steps: pre-fatigue and post-fatigue (Fig. 5B), and the post-fatigue experiment was carried out one day after the pre-fatigue experiment to avoid the influence of the previous experiment on the results.

(1) Pre-fatigue: Audio signal prompts were used to indicate the start and end of one experiment. During this experiment, the subject performed the gripping task and reached 30% of their MCV within 1 s, and then maintained it for 5 s. The whole process took 6 s, with a rest of 20 s between each action in order to avoid muscle fatigue. This task was repeated 10 times to complete the acquisition of pre-fatigue data.

(2) Post-fatigue: The above steps were repeated, while scores on the Borg Scale (Borg, 1998) of Perceived Exertion were recorded after each action, with an interval of 2 s between each movement. Only 10 data points with a Borg fatigue index (BFI) score between 14 and 19 were recorded, as shown in Table 2.

5.3. Data acquisition and pre-processing

A 64-channel (NeuSen.W64, Neuracle, China) EEG signal and three-channel EMG signal (DelsysInc, Natick, MA, USA) were collected simultaneously at a sampling frequency of 1,000 Hz. According to the international 10–20 system, we selected 10 channels (F3, F4, FC3, FC4, C3, C4, CP3, CP4, P3, and P4), after removing the bad channels, from 64 EEG channels. EMG signals were recorded from the flexor carpi ulnaris (FCU), flexor digitorum superficialis (FDS), and flexor carpi radialis (FCR). The skin surface was cleaned with alcohol before connecting the electrodes.

The EEGLAB toolbox (Delorme and Makeig, 2004) was used to pre-process the EEG signal re-referenced to the common average reference. Independent component analysis was used to remove artifacts, such as eye movement. The combination of empirical mode decomposition (EMD) and wavelet threshold was used to remove noise in the EMG signals. Through band-pass filtering, both EEG and EMG were divided into beta band (12–30 Hz) and gamma band (30–45 Hz) for further analysis.

5.4. Data analysis

5.4.1. Symbolic transfer entropy

Staniek and Lehnertz (2008) proposed STE by combining transfer entropy (TE) with the concept of symbolization. Symbolizing the signal before TE calculation can capture large-scale dynamic characteristics and reduce the influence of noise. Given the time series $X = \{x_1, x_2, \ldots x_i\}$ and $Y = \{y_1, y_2, \ldots y_i\}$, where i is the sampling point. The symbolization process (Gao et al., 2018) is defined as:

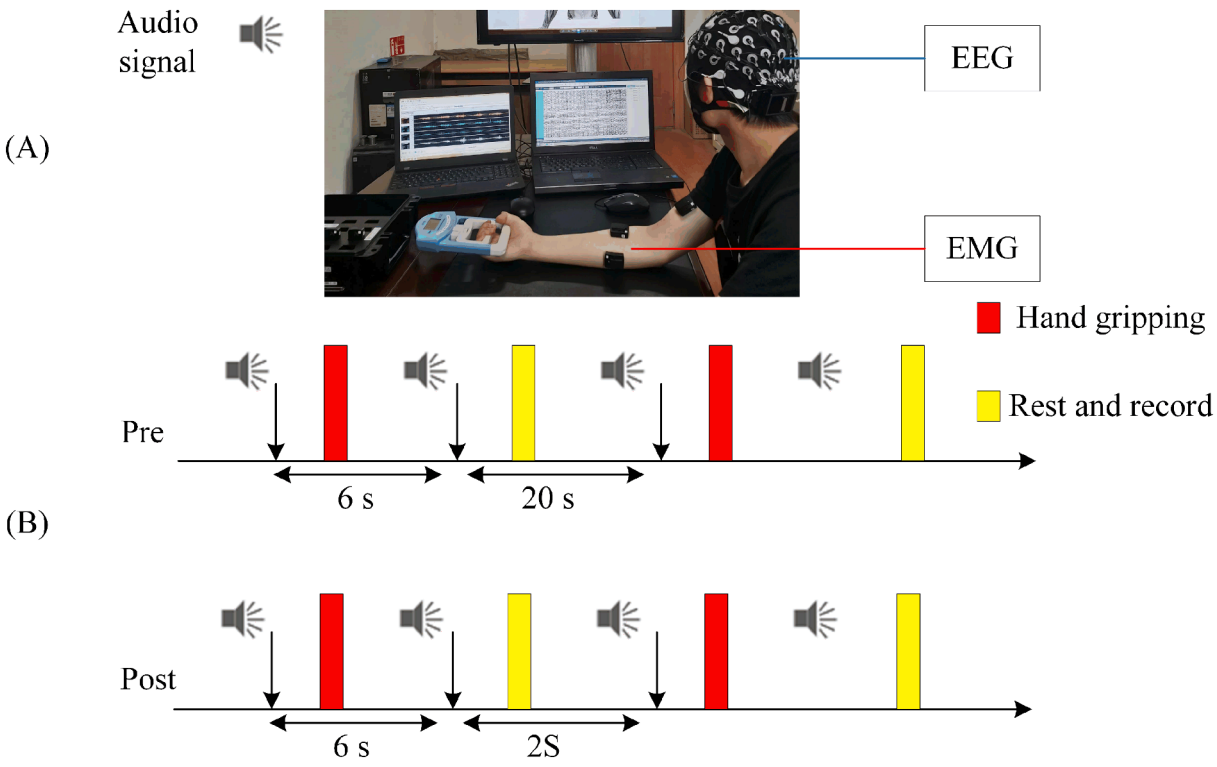

Fig. 5. Experimental setup and paradigm. (A) Experimental environment and posture of the subjects in the experiment. Audio signal prompts were used to indicate the start and end of one experiment; (B) Flow of the experimental task. Each experiment took 6 s. For pre-fatigue experiment, the interval between each experiment was 20 s; for post-fatigue experiment, the interval between each experiment was 2 s, and the Borg fatigue index was recorded after each experiment.

$$S(i)=\begin{cases} -\frac{p}{2}, & min(x)\leqslant x(i)<min(x)+delta \\ -\frac{p}{2}+0.5, & min(x)+delta\leqslant x(i)<min(x)+2{*}delta \\ \cdots\cdots & \\ 0, & min(x)+(p-1){*}delta\leqslant x(i)<min(x)+p{*}delta \\ \cdots\cdots & \\ \frac{p}{2}-0.5, & max(x)-2{*}delta\leqslant x(i)<max(x)-delta \\ \frac{p}{2}, & max(x)-delta\leqslant x(i)<max(x) \end{cases} \quad (1)$$

where S(i) represents the symbolized sequence, min and max represent the minimum and maximum values of the time series respectively, delta was defined as $delta=\frac{max(x)-min(x)}{p-1}$, the symbolic scale parameter was denoted as p. To select an appropriate scale parameter, the objective function G (Gao et al., 2018) was defined as: $G=M-S$, where M and S represent the average values and standard deviation of the STE, respectively. The scale parameter was determined as the abscissa when G reached its peak. Fig. 6 shows the average STE from C3 to FDS for each scale in the interval 5–50 with a step of 5. The blue line represents the average values of STE and the red line represents the value of the objective function G. The short vertical lines denote the standard deviation of the STE. Based on the red line, the scale parameter of STE was set to 45 in the beta band and 40 in the gamma band.

Symbolized signal $X^s=\{x_1^s,x_2^s,\ldots x_i^s\}$ and $Y^s=\{y_1^s,y_2^s,\ldots y_i^s\}$ were obtained after symbolization. Then the STE of X to Y was defined as:

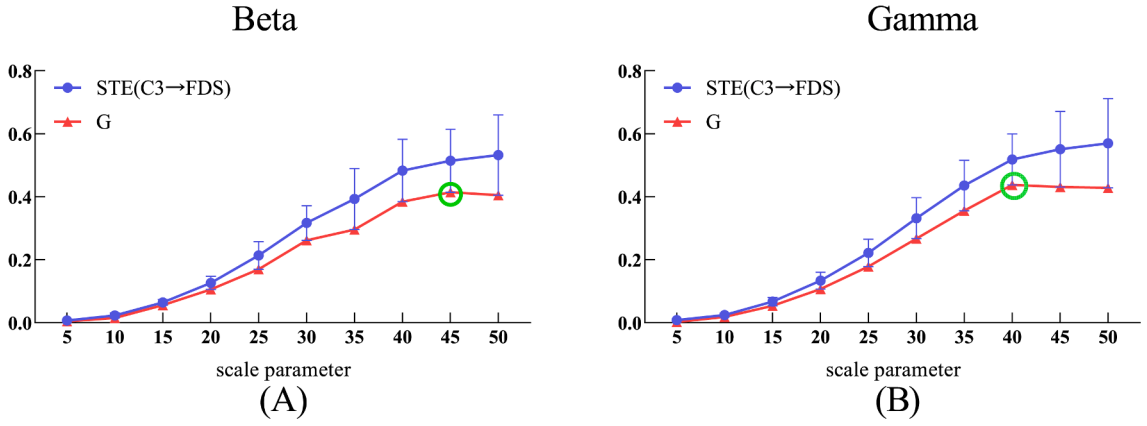

Fig. 6. Determination of the time scale parameter in symbolization. (A) Average values of the STE and G during pre-fatigue in beta band; (B) Average values of the STE and G during pre-fatigue in gamma band. The blue line represents the average values of STE from C3 to FDS. The red line represents the value of the objective function G. The short vertical lines denote the standard deviation of the STE. The green circle marks the maximum value of the objective function G.

$$STE_{X\to Y} = \sum_{y_{i+1}^s, y_i^s, x_i^s} p(y_{i+1}^s, y_i^s, x_i^s) log_2 \left(\frac{p(y_{i+1}^s, y_i^s, x_i^s) p(y_i^s)}{p(x_i^s, y_i^s) p(y_{i+1}^s, y_i^s)} \right) \quad (2)$$

where $p(\cdot)$ represents the probability distribution. The STE of Y to X can be calculated as the same way. Under this measure, the value of STE indicates the strength of the coupling relationship between X and Y. Note that when X and Y are the same, STE = 0.

In this study, we calculated the STE of EEG-EEG, EMG-EMG and EEG-EMG in two frequency bands (beta band and gamma band). The STE of EMG-EMG had a 3*3 matrix, the STE of EEG-EEG had a 10*10 matrix, the STE of EEG-EMG had a 10*3 matrix (EEG → EMG) and a 3*10 matrix (EMG → EEG), and finally we integrated these STE matrices into a 13*13 weighted adjacency matrix. The matrix element represents the STE value from the row channel to the column channel.

5.4.2. Threshold determination

To binarize the weighted adjacency matrix, a cost efficiency (Ce) threshold (th) was adopted:

$$th = max\{Ce\} = max\{E_g - D\} \quad (3)$$

Here D is the network density, which is defined as the ratio of the actual number of edges to the number of all possible edges; and E_g represents the global efficiency:

$$E_g = \frac{1}{N(N-1)} \sum_{i \neq j}^{N} \frac{1}{L_{i,j}} \quad (4)$$

where $L_{i,j}$ represents the shortest path length between the nodes i and j, N is the number of nodes in the graph.

The threshold that maximizes cost efficiency was used to binarize the weighted matrix. We set an individualized threshold for each adjacency matrix, which resulted in a directed binary adjacency matrix for further graph analysis.

5.4.3. Graph analysis

In this study, the degree, local efficiency, clustering coefficient, and small-world index of the binary cortical-muscle network were calculated.

For the analyzed network, the in-degree of a node represented the number of edges directed towards this node from other nodes, and the out-degree represented the number of edges directed towards other nodes from this node.

The local efficiency was defined as the average efficiency of the local sub-graphs, and E_l was defined as $E_l = \frac{1}{N}\sum_{i=1}^{N} E_g(A_i)$, where $E_g(A_i)$ represents the global efficiency of A_i (the sub-graph of the neighbors of the node i), which can be obtained by Eq. (4).

The clustering coefficient represented the possibility that the neighbors of a node became neighbors of each other, and the local clustering coefficient of node i was defined as $C_i = \frac{2B_i}{K_i(K_i - 1)}$, where B_i represented the number of connections between neighbor nodes of node i, and K_i represented the number of neighbor nodes of node i.

The small-world index is defined as:

$$\sigma = \frac{C_{real}}{C_{random}} \Big/ \frac{L_{real}}{L_{random}} \quad (5)$$

Where C_{real} and C_{random} are the network clustering coefficient of the analyzed network and the random network, respectively; L_{real} and L_{random} are the global shortest path length of the analyzed network and the random network, respectively. The network clustering coefficient can be calculated by $C = \frac{1}{N}\sum_{i=1}^{N} C_i$, and the global shortest path length can be calculated by $L = \frac{1}{E_g}$. If the small-world index greater than 1 σ, this means that the network has the small-world property.

5.5. Statistical analysis and classification

To evaluate the statistical differences in the STE, degrees, local efficiency, clustering coefficient, and small-world properties before and after fatigue, paired Student's t-tests were used. An α-level of 5% was chosen for further statistical analyses. Multiple comparison correction based on the Benjamini-Hockberg method was performed to control the false discovery rate.

The degree, efficiency, and clustering coefficient have been calculated for each node in each cortical-muscle network, resulting in 3*13 feature matrix (3 types and 13 channels) for each frequency band. Subsequently, according to the 10-fold cross-validation, these feature matrices were taken as input of the SVM algorithm to train the classifier for the final fatigue recognition. The SVM classifier was implemented by the LIBSVM toolbox in MATLAB and parameters were set to default values. Similarly, we also calculated these features of brain network (3*10 feature matrix) for comparison.

CRediT authorship contribution statement

Xugang Xi: Conceptualization, Funding acquisition, Writing - review & editing. **Shaojun Pi:** Methodology, Software, Writing - original draft. **Yun-Bo Zhao:** Validation, Formal analysis, Resources, Visualization. **Huijiao Wang:** Investigation, Data curation. **Zhizeng Luo:** Supervision, Project administration.

Declaration of Competing Interest

The authors declare that they have no known competing financial interests or personal relationships that could have appeared to influence the work reported in this paper.

Acknowledgments

This work was supported by the National Natural Science Foundation of China (Nos. 61971169, and 60903084), Provincial Key R&D Program of Zhejiang Province (No.2021C03031), Zhejiang Natural Science Foundation of China (No. LY17F030021).

References

Ament, W., Verkerke, G.J., 2009. Exercise and fatigue. Sport. Med. 39, 389–422.
Avena-Koenigsberger, A., Misic, B., Sporns, O., 2018. Communication dynamics in complex brain networks. Nat. Rev. Neurosci. 19, 17.
Baars, B.J., Gage, N.M., 2010. Cognition, Brain, and Consciousness: Introduction to Cognitive Neuroscience. Academic Press.
Belardinelli, P., Laer, L., Ortiz, E., Braun, C., Gharabaghi, A., 2017. Plasticity of premotor cortico-muscular coherence in severely impaired stroke patients with hand paralysis. NeuroImage Clin. 14, 726–733.
Borg, G., 1998. Borg's perceived exertion and pain scales. Hum. Kinet.
Busan, P., Monti, F., Semenic, M., Pizzolato, G., Battaglini, P.P., 2009. Parieto-occipital cortex and planning of reaching movements: a transcranial magnetic stimulation study. Behav. Brain Res. 201, 112–119. https://doi.org/https://doi.org/10.1016/j.bbr.2009.01.040.
Chakarov, V., Naranjo, J.R., Schulte-Mönting, J., Omlor, W., Huethe, F., Kristeva, R., 2009. Beta-range EEG-EMG coherence with isometric compensation for increasing modulated low-level forces. J. Neurophysiol. 102, 1115–1120.
Contessa, P., De Luca, C.J., Kline, J.C., 2016. The compensatory interaction between motor unit firing behavior and muscle force during fatigue. J. Neurophysiol. 116, 1579–1585.
Conway, B.A., Halliday, D.M., Shahani, U., Maas, P., Weir, A.I., Rosenberg, J.R., Farmer, S.F., 1995. Common frequency components identified from correlations between magnetic recordings of cortical activity and the electromyogram in man. J. Physiol.-London 483, 35.
Delorme, A., Makeig, S., 2004. EEGLAB: an open source toolbox for analysis of single-trial EEG dynamics including independent component analysis. J. Neurosci. Methods 134, 9–21.
Di Fronso, S., Tamburro, G., Robazza, C., Bortoli, L., Comani, S., Bertollo, M., 2018. Focusing attention on muscle exertion increases EEG coherence in an endurance cycling task. Front. Psychol. 9, 1249.
Gandevia, S.C., 2001. Spinal and supraspinal factors in human muscle fatigue. Physiol. Rev.

Gao, Y., Ren, L., Li, R., Zhang, Y., 2018. Electroencephalogram–electromyography coupling analysis in stroke based on symbolic transfer entropy. Front. Neurol. 8, 716.
Karthick, P.A., Venugopal, G., Ramakrishnan, S., 2016. Analysis of muscle fatigue progression using cyclostationary property of surface electromyography signals. J. Med. Syst. 40, 28.
Liu, J.Z., Lewandowski, B., Karakasis, C., Yao, B., Siemionow, V., Sahgal, V., Yue, G.H., 2007. Shifting of activation center in the brain during muscle fatigue: an explanation of minimal central fatigue? Neuroimage 35, 299–307.
Liu, J.Z., Yao, B., Siemionow, V., Sahgal, V., Wang, X., Sun, J., Yue, G.H., 2005. Fatigue induces greater brain signal reduction during sustained than preparation phase of maximal voluntary contraction. Brain Res. 1057, 113–126.
Martínez-Aguilar, G.M., Gutiérrez, D., 2019. Using cortico-muscular and cortico-cardiac coherence to study the role of the brain in the development of muscular fatigue. Biomed. Signal Process. Control 48, 153–160.
Mima, T., Steger, J., Schulman, A.E., Gerloff, C., Hallett, M., 2000. Electroencephalographic measurement of motor cortex control of muscle activity in humans. Clin. Neurophysiol. 111, 326–337.
Mima, T., Toma, K., Koshy, B., Hallett, M., 2001. Coherence between cortical and muscular activities after subcortical stroke. Stroke 32, 2597–2601.
Muldoon, S.F., Bridgeford, E.W., Bassett, D.S., 2016. Small-world propensity and weighted brain networks. Sci. Rep. 6, 22057.
Nielsen, B., Hyldig, T., Bidstrup, F., Gonzalez-Alonso, J., Christoffersen, G.R.J., 2001. Brain activity and fatigue during prolonged exercise in the heat. Pflügers Arch. 442, 41–48.
Omlor, W., Patino, L., Hepp-Reymond, M.-C., Kristeva, R., 2007. Gamma-range corticomuscular coherence during dynamic force output. Neuroimage 34, 1191–1198.
Pellicano, C., Gallo, A., Li, X., Ikonomidou, V.N., Evangelou, I.E., Ohayon, J.M., Stern, S. K., Ehrmantraut, M., Cantor, F., McFarland, H.F., 2010. Relationship of cortical atrophy to fatigue in patients with multiple sclerosis. Arch. Neurol. 67, 447–453.
Sheffield, J.M., Kandala, S., Tamminga, C.A., Pearlson, G.D., Keshavan, M.S., Sweeney, J. A., Clementz, B.A., Lerman-Sinkoff, D.B., Hill, S.K., Barch, D.M., 2017. Transdiagnostic associations between functional brain network integrity and cognition. JAMA Psychiatr. 74, 605–613.
Staniek, M., Lehnertz, K., 2008. Symbolic transfer entropy. Phys. Rev. Lett. 100, 158101.
Strogatz, S.H., 2001. Exploring complex networks. Nature 410, 268–276.
Wan, J., Qin, Z., Wang, P., Sun, Y., Liu, X., 2017. Muscle fatigue: general understanding and treatment. Exp. Mol. Med. 49, e384–e384.
Wang, L., Lu, A., Zhang, S., Niu, W., Zheng, F., Gong, M., 2015. Fatigue-related electromyographic coherence and phase synchronization analysis between antagonistic elbow muscles. Exp. brain Res. 233, 971–982.
Wang, M.-Y., Lu, F.-M., Hu, Z., Zhang, J., Yuan, Z., 2018. Optical mapping of prefrontal brain connectivity and activation during emotion anticipation. Behav. Brain Res. 350, 122–128.
Watts, D.J., Strogatz, S.H., 1998. Collective dynamics of 'small-world'networks. Nature 393, 440–442.
Yang, Q., Fang, Y., Sun, C.-K., Siemionow, V., Ranganathan, V.K., Khoshknabi, D., Davis, M.P., Walsh, D., Sahgal, V., Yue, G.H., 2009. Weakening of functional corticomuscular coupling during muscle fatigue. Brain Res. 1250, 101–112.
Yang, Q., Siemionow, V., Yao, W., Sahgal, V., Yue, G.H., 2010. Single-trial EEG-EMG coherence analysis reveals muscle fatigue-related progressive alterations in corticomuscular coupling. IEEE Trans. Neural Syst. Rehabil. Eng. 18, 97–106.
Yao, W., Wang, J., 2017. Multi-scale symbolic transfer entropy analysis of EEG. Phys. A Stat. Mech. its Appl. 484, 276–281.
Yoshida, T., Masani, K., Zabjek, K., Chen, R., Popovic, M.R., 2017. Dynamic increase in corticomuscular coherence during bilateral, cyclical ankle movements. Front. Hum. Neurosci. 11, 155.